Laser and Particle Beams (2008), *26*, 41–50. Printed in the USA.
Copyright © 2008 Cambridge University Press 0263-0346/08 $20.00
doi: 10.1017/S0263034608000062

Spectroscopic studies of Ca plasma generated by the fundamental, second, and third harmonics of a Nd:YAG laser

S. HAFEEZ, N.M. SHAIKH,* AND M.A. BAIG

Atomic and Molecular Physics Laboratory, Department of Physics, Quaid-i-Azam University, Islamabad, Pakistan

(RECEIVED 22 May 2007; ACCEPTED 24 January 2008)

Abstract

The ablation of calcium sample has been studied by the optical emission spectroscopy of the evolving plasma using the fundamental, second, and third harmonic of a Nd:YAG laser, which reveals numerous transitions due to neutral and singly ionized calcium. The measurements have been performed to determine the electron temperature and electron number density and their spatial behavior. In addition, the behavior of the electron temperature and number density as a function of laser irradiance and ambient gas pressure has been studied. The processes of laser photon absorption in the plasma through inverse bremsstrahlung and photoionization have also been discussed.

Keywords: Boltzmann plot; Calcium; Laser-ablation; Plasma; Stark broadening

1. INTRODUCTION

Laser ablation is an exciting field of study both theoretically and experimentally because of its significance in deposition of thin films (Veiko *et al.*, 2006) and vaporization of sample material for spectro-chemical analysis (Wieger *et al.*, 2006; Schade *et al.*, 2006). In the laser induced breakdown spectroscopy (LIBS) technique, a laser pulse is used to form micro plasma on the surface of the sample being analyzed. In metals, the light is absorbed *via* interaction with the electrons which are raised to the higher energy states. The excited electrons collide with the lattice phonons, thereby transferring the absorbed energy to the lattice (Bogaerts *et al.*, 2003; Lam *et al.*, 2007; Ozaki *et al.*, 2007). A portion of the sample is vaporized during the laser pulse to form plasma of the sample constituents containing electronically excited atomic species. Initially the laser pulse deposits energy at the solid surface, this local heating drives the hydrodynamic pressure, which causes both the ejection of the hot matter away from the target and launching of shock waves into the solid sample (Vidal *et al.*, 2001; Schaumann *et al.*, 2005).

LIBS have been used extensively in qualitative and quantitative studies for the analysis of elemental species in solid, liquid, gases, and aerosol substances. Laser ablation can provide rapid chemical analysis either in laboratory or in fields. Extensive studies have been devoted in the field of LIBS and mostly the fundamental parameters have been extracted from the spectroscopic analysis of the transition lines. The plasma parameters are heavily dependent on the irradiation conditions such as incident laser fluence, spot size, pressure, and laser wavelength (Martin *et al.*, 1992; D'Couto & Babu, 1994; Abdellatif & Imam, 2002; Zbroniec *et al.*, 2004; Chen & Bogaerts, 2005; Shaikh *et al.*, 2006*a*, 2006*b*, 2006*c*, 2007). Laser induced breakdown spectroscopy is the only technique that can be used to chemically characterize any sample metals, liquid, gases, rocks, glasses, plants, bones, teeth, etc (Ying *et al.*, 2003). This technique can also be used for analysis in environment, industry, art, medical applications, and geology (Wieger *et al.*, 2006; Thareja *et al.*, 2006).

In spite of many applications, the exact mechanism of laser ablation is still not fully understood. Moreover, different kinds of mechanisms can play a role depending on the type of the material, the laser irradiance, the laser pulse duration, etc. In literature, a variety of models for laser ablation are available operating in different regimes of wavelengths (1064 nm, 532 nm, 355 nm, and 308 nm), laser irradiance and pulse duration (fs, ps, ns) target materials and gas environment (Bulgakov & Bulgakov, 1998; Colonna *et al.*, 2001; Laville *et al.*, 2004; Gomes *et al.*, 2004; Capitelli *et al.*, 2004; Chen & Bogaerts, 2005; Bogaerts *et al.*, 2006; Wang *et al.*, 2007; Bussoli *et al.*, 2007; Bashir *et al.* 2007). A number of studies concerning the influence of

Address correspondence and reprint requests to: M. A. Baig, Atomic and Molecular Physics Laboratory, Department of Physics, Quaid-i-Azam University, 45320 Islamabad, Pakistan. E-mail: baig@qau.edu.pk
*Current Address: Institute of Physics, University of Sindh, Jamshoro, Pakistan.

https://doi.org/10.1017/S0263034608000062 Published online by Cambridge University Press

various ambient atmospheres have been devoted to find optimum atmospheric conditions for practical application and spectro-chemical analysis (Lee *et al.*, 1992; Cristoforetti *et al.*, 2004; Shaikh *et al.*, 2006*a*, 2006*b*, 2006*c*). Pulsed laser ablation of a solid target in an ambient gas has proven to be an attractive technique for the production of thin films in a wide variety of materials (Trusso *et al.*, 2005). The presence of the background gas complicates the expansion of the plume as compared to the expansion in vacuum. A wide variety of gas dynamic models have been recently proposed to understand these complexities (Bulgakov & Bulgakov, 1998; Colona *et al.*, 2001).

Calcium is the fifth element and the third most abundant metal in the earth crust and is essential for the life of plants, animals, and humans. It is present in the bones, teeth, egg's shell and soil, and its detection is important in wide applications ranging from ore analysis, environmental effects, health effects, and coal industry. It is one of the main components of soils and plays an important role in determining their cohesibility and fertility. However, little information is available for the calcium plasma parameters, like electron temperature, and electron number density. Bustamante *et al.* (2002) used the laser induced breakdown spectroscopy technique for the analysis of Ca in a soil depth profile from Patagonia, Argentina. Maravelaki-Kalaitzaki *et al.* (2001) employed LIBS to characterize the encrustation on the marble. Barklem and Mara Mon (1998) studied the broadening of Ca II, Mg II, and Ba II spectral lines employing the theory of Anste and O'Mara (1991, 1995) and calculated the broadening cross-section for strong lines of these elements. The spectral profiles of the Ca and Rb transition lines have been studied by Gornushkin *et al.* (1999) in a laser induced plasma as a function of pressure, and delay using a Nd:YAG laser at 1064 nm. Body & Chadwick (2001) presented new instrumentation variation on LIBS and used it for the analysis of coal detecting Al, Si, Mg, Ca, Fe, Na, K, C, and H as its key inorganic components.

In this paper, based on the results of quantitative plasma diagnostics, plasma parameters have been estimated. The aim of the experiment was to study the effect of laser energy and ambient atmosphere on the spectral line intensities as well as on the plasma parameters. The Boltzmann plot method is used to estimate the electron temperature, while Stark broadened profile of the singly ionized calcium transition is used for the electron number density measurement.

2. EXPERIMENTAL SETUP

The experimental setup is similar as described in our pervious work (Shaikh *et al.*, 2006*a*, 2006*b*, 2006*c*, 2007) and shown in Figure 1. A Q-switched Nd:YAG pulsed laser (Brilliant, Quantel) at its fundamental (1064 nm), second harmonic (532 nm), and third harmonic (355 nm) was used to ablate the target. The laser beam having pulse duration 5 ns and 10 Hz repetition rate was focused on the target using a convex lens of 20 cm focal length. The target in the form of a disc was placed in a chamber provided with two optical windows, one for the laser irradiance and a side window for the spectroscopic observation of the plasma. The target was rotated to avoid the non-uniform pitting of the target. The spectra were obtained by averaging 10 data of single laser shot under identical experimental conditions. The radiation emitted by the plasma were collected by a fiber optics (high-OH, core diameter: 600 μm) having a collimating lens (0–45°) field of view placed at right angle to the direction of the laser beam. This optical fiber was connected with the LIBS2000 detection system (Ocean Optics. Inc.) to measure the plasma emission. The LIBS2000 detection system is equipped with five spectrometers each having slit width of 5 μm, covering the range between 200–700 nm. Each spectrometer has 2048 element linear charge coupled devices (CCD) array and an optical resolution of ≈0.05 nm. In order to record the emission spectrum, the LIBS2000 detection system was synchronized with the Q-switch of the Nd:YAG laser. The flash lamp out of the laser triggered the detection system through a four channel digital delay/pulse generator (SRS DG 535). The LIBS2000 detection system triggered the Q-switch of the Nd:YAG laser. The laser pulse energy was varied through the Ocean Optics, Inc. laser induced breakdown spectroscopy (OOILIBS) software. The system has been calibrated in wavelength by recording the well-known lines of neon, argon, and mercury covering the wavelength range 200–720 nm. The uncertainty in the measured wavelengths is ≈ 0.02 nm. All the five spectrometers installed in the LIBS 2000 have been manufacturer calibrated in efficiency using the DH-2000-CAL standard light source. The data acquired simultaneously by all the five spectrometers were stored on a PC through the OOILIBS software for subsequent analysis.

3. RESULT AND DISCUSSIONS

3.1. Description of the Observed Spectra

In this work, we have studied the plasma emission generated by the fundamental (1064 nm), second harmonic (532 nm), and third harmonic (355 nm) of the Q-switched Nd:YAG laser. In the first set of experiments, the 1064 nm, 532 nm, and 355 nm lasers are focused on the calcium surface and the emission spectra of the respective plasma are recorded. The emission spectra of the laser produced calcium plasma are reproduced in Figures 2a and 2b covering the spectral region from 300–650 nm. In order to understand the entire spectrum, it is pertinent to divide the spectrum belonging to the ionic and neutral atomic transitions. The spectrum between 300–400 nm predominantly belongs to the ionic transitions connecting the 4p first excited state to the 4s lower state, 5s to 4p, and 4d to 4p, excited states of the singly ionized calcium. The lines below 400 nm reveal doublet structure and most intense doublet lies around 390 nm which is designated as $4p\ ^2P_{1/2,3/2} \rightarrow 4s\ ^2S_{1/2}$ at 393.47 nm and 396.95 nm, the doublet structure around

https://doi.org/10.1017/S0263034608000062 Published online by Cambridge University Press

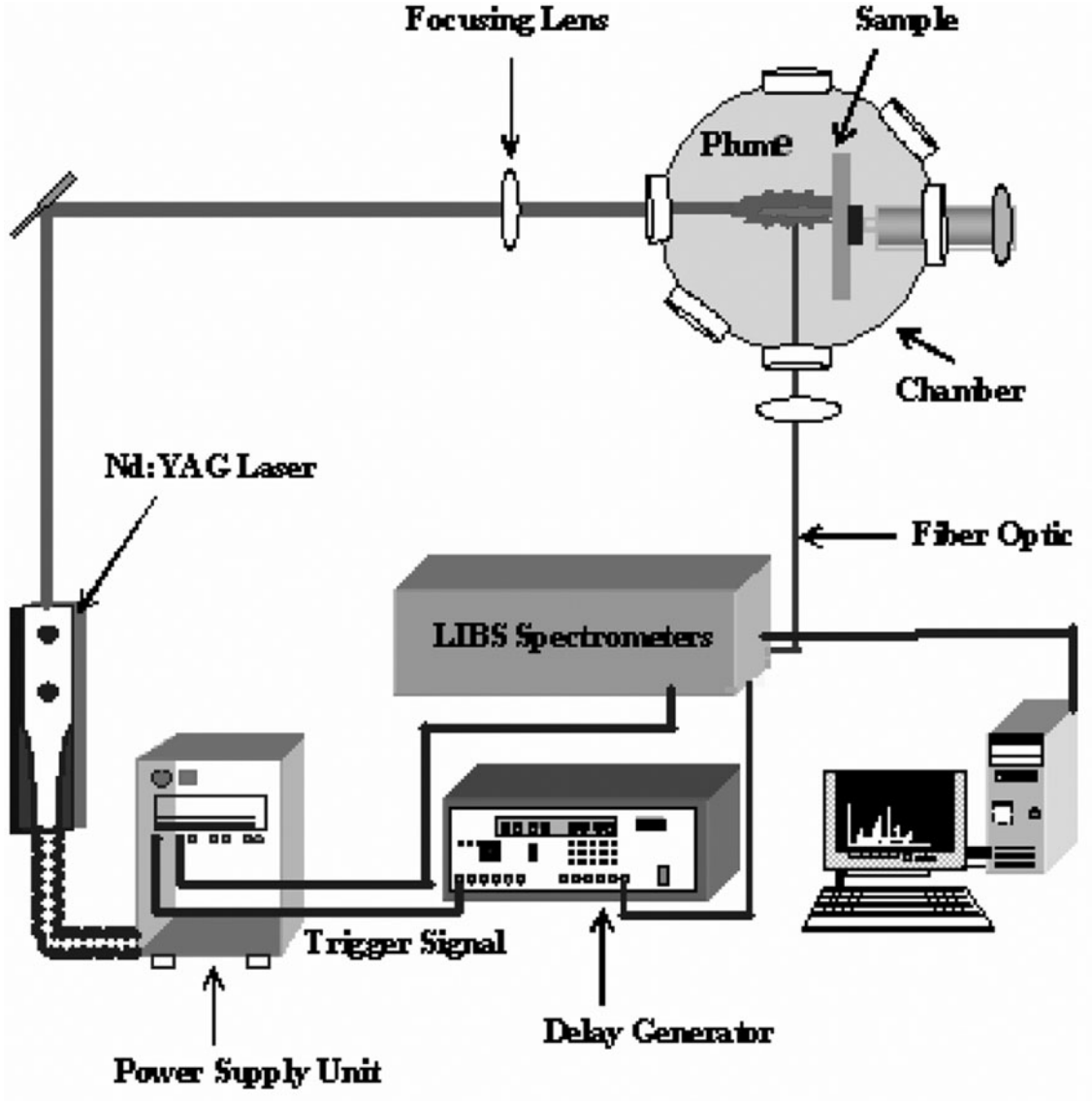

Fig. 1. Schematic diagram of the experimental setup.

370 nm originates from the 4s $^2S_{1/2} \rightarrow 4p\ ^2P_{1/2,3/2}$ transitions at 370.6 nm and 373.6 nm. The well separated structure around 320 nm is due to the 4d $^2D_{3/2} \rightarrow 4p\ ^2P_{1/2,3/2}$ transitions at 315.97 nm and 318.02 nm. In accordance to the selection rules, three lines are expected in this multiplet but only two have been detected. The third line is expected to lie at 318.02 nm, but it is too week to be detected in the present work. Because of the low ionization potential of calcium the lines of calcium ions are very intense.

The neutral calcium transitions 4s4d $^3D_{2,1} \rightarrow 4s4p\ ^3P_{1,0}$ are observed around 445 nm and 4s5s $^3S_1 \rightarrow 4s4p\ ^3P_{2,1,0}$ at 314 nm. Some transitions are observed terminating at the 4s3d $^3D_{2,1}$ levels and a few lines have been observed due to the decay to the 4s4p $^1P_1$ level, which remains well isolated from the other structure. The resonance line of calcium 4s4p $^1P_1 \rightarrow 4s^2\ ^1S_0$ at 422 nm is also prominent in the observed spectra.

3.2. Determination of Electron Temperature and Electron Number Density

The key parameters of the laser ablated plume are density and plasma temperature. These parameters have been estimated under the assumption of the local thermodynamic equilibrium. Once formed, the plasma is usually assumed to reach a situation of local thermodynamic equilibrium (LTE), i.e., the population density of the atomic and ionic electronic states is described by the Boltzmann distribution (Detalle *et al.*, 2001; De Giacomo *et al.*, 2003; Hafez *et al.*, 2003).

$$\frac{N(T)}{U(T)} = \frac{\lambda_{mn} I_{mn}}{g_m A_{mn}} \exp\left(\frac{E_m}{kT}\right). \quad (1)$$

Where I_{mn}, g_m, A_{mn}, and E_{mn} are the line intensity, statistical weight, transition probability, and excited level energy,

https://doi.org/10.1017/S0263034608000062 Published online by Cambridge University Press

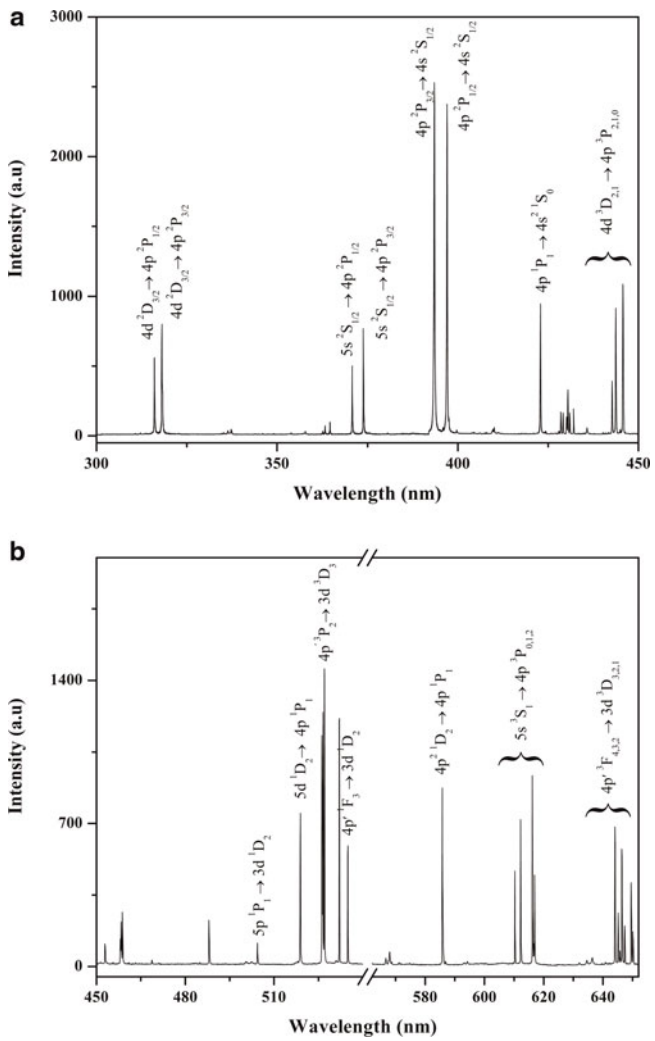

Fig. 2. The emission spectrum generated by the 1064 nm laser showing the spectral lines originating from transitions in the neutral and singly ionized calcium.

respectively, T and k are the electron temperature and Boltzmann constant, $N(T)$ is the number density and $U(T)$ is the partition function. The electron temperature has been determined, using the Boltzmann plot method, from the five spectral lines of calcium; 443.56 nm (4d $^3D_1 \rightarrow$ 4p $^3P_1$), 445.59 nm (4d $^3D_2 \rightarrow$ 4p $^3P_2$), 519.02 nm (5d $^1D_2 \rightarrow$ 4p $^1P_1$), 610.44 nm, and 612.22 nm (5s $^3S_1 \rightarrow$ 4p $^3P_{1,0}$). In Table 1, the selected transition lines are listed along with their spectroscopic parameters taken from the National Institute of Standards and Technology (NIST) data base. Similarly, in Table 2, the spectroscopic parameters of selected transition lines of Ca II are given.

The spatial behavior of the plume generated by the fundamental, second, and third harmonic of the Nd:YAG laser has been captured. In all the three laser wavelengths, the power density was adjusted at ~3×10^{10} Wcm^{-2} while the pressure was kept at 4 mbar. The electron temperature close to the surface of the calcium is found to be 16200 K, 15400 K, and 13700 K, respectively, for the 1064 nm, 532 nm, and 355 nm lasers, respectively. The high value of the electron temperature is attributed to the absorption of laser energy by the electrons *via* inverse bremsstrahlung absorption process. At these high temperatures, an appreciable flux of ions and electrons is produced. The ablation of the target accompanies a glow extending perpendicular to the target surface. The intensities of the atomic and ionic emission lines decrease as the plasma expands away from the target. The temperature decreases to 11200 K, 9500 K, and 8200 K at about 6 mm from the target as shown in Figure 3. The basis of the decrease in the temperature is the conversion of the thermal energy into the kinetic energy, resulting in an expansion and thereby cooling of the plasma.

One of the most reliable spectroscopic techniques to determine the electron density is from the Stark broadened line profiles of neutral atom or singly charged ion. The full width at half maximum (FWHM) of a spectral line can be used for the determination of electron number density, using the following relation (Harilal *et al.*, 1997; Zeng *et al.*, 2003; Colon *et al.*, 1993; Ortiz & Mayo, 2005)

$$\Delta\lambda = 2\omega\left(\frac{N_e}{10^{16}}\right) + 3.5A\left(\frac{N_e}{10^{16}}\right)^{1/4} \times \left(1 - 1.2\,N_D^{-1/3}\right)\omega\left(\frac{N_e}{10^{16}}\right). \quad (2)$$

Here ω (nm) is the electron width parameter, which is a weak function of temperature, A (nm) is the ion broadening parameter, N_e (cm^{-3}) is the electron number density, and N_D is the number of particles in the Debye sphere. The contribution due to the ion broadening is very small and can be neglected, only the first term on the right is sufficient to extract the

Table 1. *Spectroscopic parameters of the neutral calcium transitions*

Wavelength λ (nm)	Transitions	Statistical weight g_k	Statistical weight g_i	Transition Probability A (s^{-1})	Upper level Energy E_k (cm^{-1})
443.56	4d $^3D_1 \rightarrow$ 4p $^3P_1$	3	3	3.571×10^7	37748.197
445.59	4d $^3D_2 \rightarrow$ 4p $^3P_2$	5	5	2.075×10^7	37751.86
519.02	5d $^1D_2 \rightarrow$ 4p $^1P_1$	5	3	4.025×10^7	42919.074
610.44	5s $^3S_1 \rightarrow$ 4p $^3P_0$	3	1	7.686×10^6	31539.49
612.22	5s $^3S_1 \rightarrow$ 4p $^3P_1$	3	3	2.312×10^7	31539.495

https://doi.org/10.1017/S0263034608000062 Published online by Cambridge University Press

Table 2. *Spectroscopic parameters of the of the singly ionized calcium transitions*

Wavelength λ (nm)	Transitions	Statistical weight g_k	Statistical weight g_i	Transition Probability A (s^{-1})	Upper level Energy E_k (cm^{-1})
315.97	$4d\ ^2D_{3/2} \rightarrow 4p\ ^2P_{1/2}$	4	2	2.984×10^8	56839.309
318.21	$4d\ ^2D_{3/2} \rightarrow 4p\ ^2P_{3/2}$	4	4	5.87×10^7	56839.309
370.60	$4s\ ^2S_{1/2} \rightarrow 4p\ ^2P_{1/2}$	2	2	8.670×10^8	52166.93
373.60	$4s\ ^2S_{1/2} \rightarrow 4p\ ^2P_{3/2}$	2	4	1.701×10^8	52166.93
393.47	$4p\ ^2P_{1/2} \rightarrow 4s\ ^2S_{1/2}$	2	2	1.466×10^8	25414.427
396.95	$4p\ ^2P_{3/2} \rightarrow 4s\ ^2S_{1/2}$	4	2	1.444×10^8	25191.541

number density as the Stark broadened parameter is available in the literature (Griem, 1997). Besides Stark broadening, the Doppler broadening, and the finite resolution of the spectrometer might also contribute in the line broadening. The contribution of the Doppler broadening (Marr, 1968), estimated from the plasma temperature as ~0.004(1) nm, is very small and hence can safely be ignored. The instrumental width of the LIBS 2000 spectrometer system is measured as 0.05(2) nm using a narrow line width dye laser. Thus the width of the transition line mainly reflects the Stark effect.

The maximum number density under the assumption of LTE has been estimated using the McWhirter criterion (Whirter, 1965)

$$N_e(cm^{-3}) \geq 1.6 \times 10^{12} T^{1/2} (\Delta E)^3. \quad (3)$$

Here ΔE (eV) is the difference between the energy levels and T (K) is the temperature. At the highest evaluated temperature (~15000 K), Eq. (2) yields $N_e \approx 4 \times 10^{15}$ cm^{-3}, which holds the validity of LTE.

In all the three wavelengths of the Nd:YAG laser, the electron number density has been evaluated using the $4d\ ^2D_{3/2} \rightarrow 4p\ ^2P_{1/2}$ transition line of Ca II at 315.97 nm. The spatial behavior of the electron number density in the plume, shown in Figure 4, is determined using Eq. (2). When the laser is focused on the target, the ablation of the target takes place and due to the density gradient, a rapid expansion of the plasma sets in. The number density close to the target surface in the case of fundamental, second harmonic generation, and third harmonic generation are 1.3×10^{18}, 1.5×10^{18}, and 1.6×10^{18} cm^{-3}. These values decrease to 4.9×10^{17}, 6.4×10^{17}, and 7.5×10^{17} cm^{-3} at a distance of 6 mm away from the target. Hence the maximum number density is observed near the target surface which decreases as the distance from the target is increased. The decrease in the number density at larger distances is mainly due to the recombination of electrons and ions. As can be seen from Figures 3 and 4, the electron temperature and number density decreases rapidly within a short distance from the target surface, while at a larger distance, they exhibit little variation. The variation in the electron temperature is slower than that of the number density. The electron temperature and number density are different for the three wavelengths of the Nd:YAG laser, because of the difference in the energy per photon in each case.

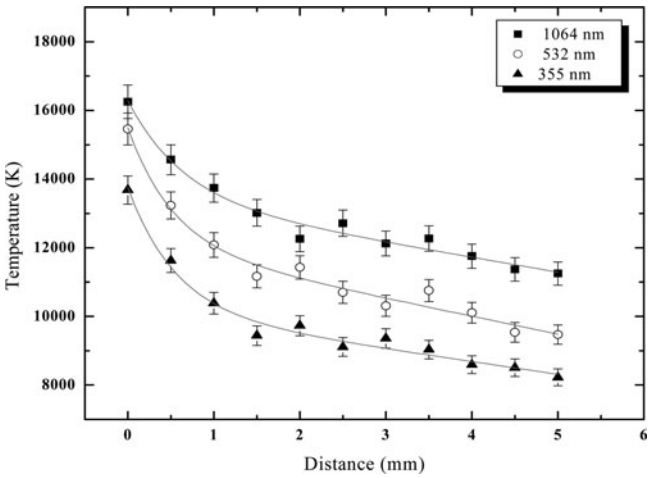

Fig. 3. Spatial behavior of the electron temperature using the 1064 nm, 532 nm, and 355 nm lasers.

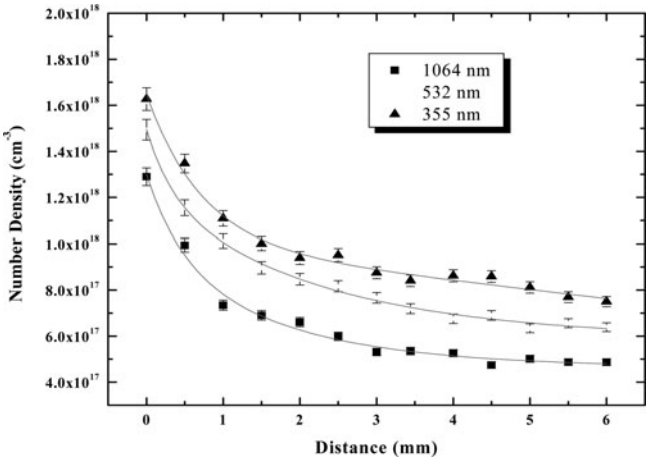

Fig. 4. Spatial behavior of the electron number density using the 1064 nm, 532 nm, and 355 nm lasers.

https://doi.org/10.1017/S0263034608000062 Published online by Cambridge University Press

Moreover, for any laser wavelength, the incident energy is totally absorbed by the plasma as an internal energy. The internal energy of the plasma is distributed in its thermal and ionization energy. It is a well-known fact that the laser wavelength influences the ablation process; however it also significantly depends on the laser irradiance. The plasma density is higher in the 355 nm lasers than in the 532 nm and 1064 nm lasers. When the 355 nm laser is used, similar energy is absorbed as compared to the 532 nm and 1064 nm lasers, but the electron density of the absorbing plasma increases, and the corresponding plasma temperature decreases. The particle density in the plasma depends on the degree of ionization, evaporation rate, and the plasma expansion velocity. Because of the high expansion velocity of the leading plasma edge, the electron density decreases, this makes the plasma transparent to the laser beam at larger distances away from the target surface. A thin region close to the surface of the target is constantly absorbing the laser radiation during the time interval of the laser pulse. The absorption in the plasma occurs by an inverse bremsstrahlung and photoionization processes.

3.3. Effect of Laser Irradiance and Laser Plasma Interaction

In the second set of the experiments, the calcium sample was irradiated by the fundamental harmonic generation (1064 nm), second harmonic generation (532 nm), and third harmonic generation (355 nm) of the Nd:YAG laser, the sample was kept at a pressure of 4 mbar, and the detector was placed at a distance of 0.5 mm from the target. In all the three wavelengths of the Nd:YAG laser, we have observed an identical trend of variation of temperature as a function of laser irradiance. The variation of electron number density also shows a similar behavior. In the three laser wavelengths, the laser irradiance ranges from 1×10^{10} to 5×10^{10} Wcm^{-2}. For the 1064 nm laser, the electron temperature varies from 10700 to 15700 K, while the electron number density varies from 6.1×10^{17} to 8.9×10^{17} cm^{-3}. For the 532 nm laser, the electron temperature varies from 8500 to 14000 K, while the electron number density varies from 6.9×10^{17} to 1.2×10^{18} cm^{-3}. Similarly for the 355 nm laser, the electron temperature varies from 6900 to 11900 K, while the electron number density varies from 9.1×10^{17} to 1.5×10^{18} cm^{-3}. The variations in the temperature and electron number density as a function of laser irradiance are shown in Figures 5 and 6, respectively. It is observed that the electron temperature increases with the increase in the laser irradiance. With the increase in the laser irradiance, the mass ablation rate also increases (Russo *et al.*, 1999), and hence the spectral line intensities and the background intensity increases as well. An increase in the number density and temperature with an increase in the laser irradiance is due to the absorption or reflection of the laser photon by the plasma. More important is the subsequent laser pulse energy transfer to the sample and plasma particles.

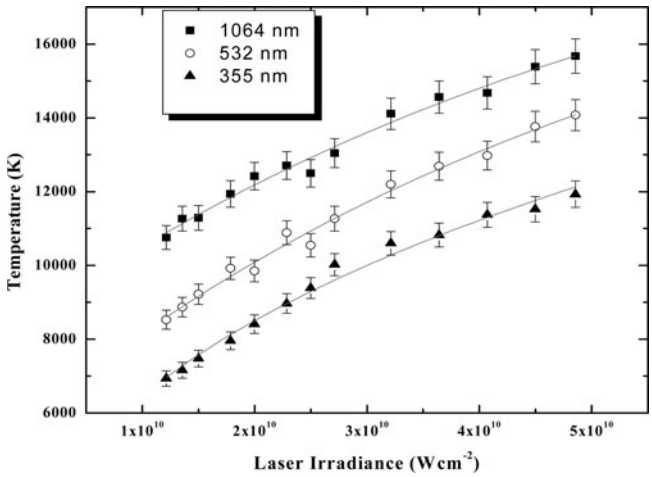

Fig. 5. Variation of the electron temperature with the laser irradiance using the 1064 nm, 532 nm, and 355 nm lasers.

As plasma is formed, its electron density N_e and thus the plasma frequency ω_p are increasing. As soon as ω_p becomes larger than the laser frequency, plasma starts to reflect the laser radiation (plasma shielding), becoming opaque. Thus a very little of the remaining laser energy participates in the evaporation and ionization process. An ultraviolet laser is more efficient to penetrate the plasma and subsequently producing analytic-richer plasma. Depending on the laser pulse energy, the plasma reflectivity with ultraviolet is 20% and for infrared reduces to 7% (Asimellis *et al.*, 2006). In order to analyze the absorption mechanisms of the laser induced plasma, its thermodynamic properties including temperature and number density are to be known. In our experiments, for all the three wavelengths of the Nd:YAG laser (1064 nm, 532 nm, and 355 nm), the corresponding frequencies are 2.8×10^{14} Hz, 5.6×10^{14} Hz, and

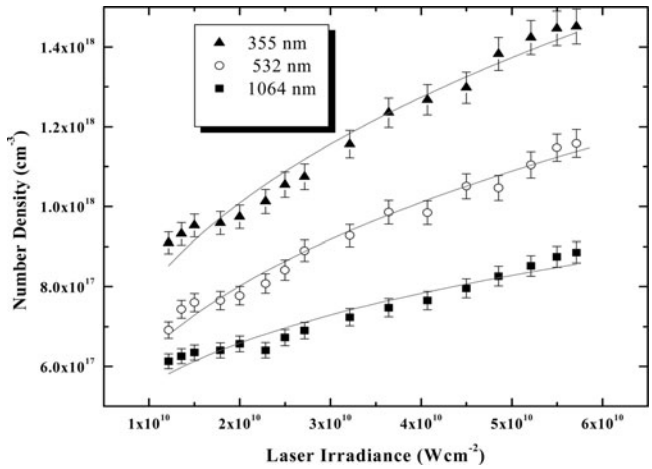

Fig. 6. Variation of the electron number density with the laser irradiance using the 1064 nm, 532 nm, and 355 nm lasers.

https://doi.org/10.1017/S0263034608000062 Published online by Cambridge University Press

8.5×10^{14} Hz. The plasma frequency is estimated from the relation $\nu_p = 8.9 \times 10^3 N_e^{0.5}$ (Singh *et al.*, 1990). The electron number density is ~1×10^{18} cm^{-3} and υ_p ~9×10^{12} Hz, which is much lower than the laser frequency. Therefore, the loss of energy due to the reflection of the laser from the plasma is negligible.

There are two dominant photon absorption processes occurring in plasma. One is the inverse bremsstrahlung absorption by which the free electrons gain kinetic energy from the laser beam, thus promoting plume ionization and excitation through collisions with the excited and ground state neutrals. The inverse bremsstrahlung absorption is estimated using the relation (Chang & Warner, 1996)

$$\alpha_{ib}(cm^{-1}) \approx 1.37 \times 10^{-35} \lambda^3 N_e^2 T_e^{-1/2}. \quad (4)$$

Where λ (μm) is the wavelength of the laser, T_e (K) is the electron temperature, and N_e (cm^{-3}) is the electron density. Because of its λ^3 dependence, the ion beam process is more efficient in case of 1064 nm as compared to 532 nm and 355 nm lasers as shown in Figure 7. Higher laser irradiance results in a higher vapor density and temperature, resulting in more excited atoms, and hence more laser photon absorption. Hence there will be a decrease in the evaporation process from the target. With increasing laser irradiance more free electrons, ions, and excited atoms are generated. In an intense laser field, the free electrons can gain sufficient energy through the inverse bremsstrahlung absorption; these electrons will ionize or excite the atoms through collisions and resulting in an increase in the absorption of laser energy.

The second mechanism is photo-ionization or multi-photon ionization of the excited or the ground state atoms. In calcium, the lowest term of the triplet system 4s4p $^3P_0$ is metastable, the first excited state lies 2.9 eV above the ground state, where as its ionization potential is 6.11 eV. The energy of the photon in the case of 355 nm, 532 nm, and 1064 nm laser is 3.5 eV, 2.3 eV, and 1.16 eV, respectively. Hence in the case of the 532 nm and 1064 nm lasers, multi-photon ionization is required whereas photo-ionization is possible for the 355 nm laser. The photo-ionization absorption coefficient α_{PI} (cm^{-1}) can be approximated as described by Harilal *et al.* (1997) and Amorusso *et al.* (1999). The contribution of photo-inizotion (PI) absorption coefficient is shown in the Figure 8. The power absorbed by the plasma from the incident laser beam at any time is given by Singh *et al.* (1990)

$$P_{abs} = P(1 - e^{-X\alpha_P}). \quad (5)$$

Where α_p is the absorption coefficient of the plasma, P is the power of the laser beam, and X is the dimension of the plasma in the direction perpendicular to the laser beam. The rate of electron impact excitation τ_{ex}^{-1} can be expressed as (Amoruso *et al.*, 1999)

$$\tau_{ex}^{-1} \approx 6.6 \times 10^{-10} T_e^{0.5} (2 + \frac{\varepsilon*}{T_e}) \exp(-\frac{\varepsilon*}{T_e}) N_e. \quad (6)$$

For N_e ~8.3×10^{17} cm^{-3}, $T_e = 1.6$ eV, and $\varepsilon* = 2.9$ eV, the τ_{ex} turns out to be ~0.4 ns which is sufficiently short time to enhance the excited neutral density. Thus an increase in the electron density caused by the inverse Bremsstrahlung (IB) process produces an increase in the excited neutral density which can trigger an electron avalanche.

3.4. Influence of Ambient Conditions

To study the effect of the ambient pressure on the emission signal strength, the spectra with varying pressure have been recorded using the 1064 nm laser. The emission lines pro-

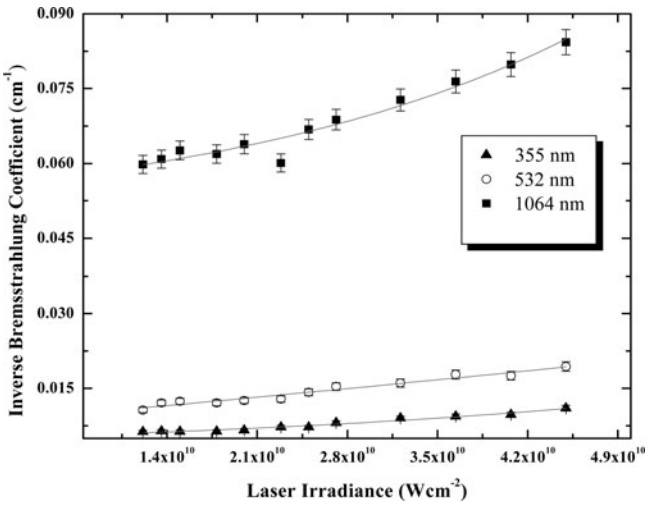

Fig. 7. Variation of the calculated inverse bremsstrahlung absorption α_{IB} with the laser irradiance at 1064 nm, 532 nm, and 355 nm lasers.

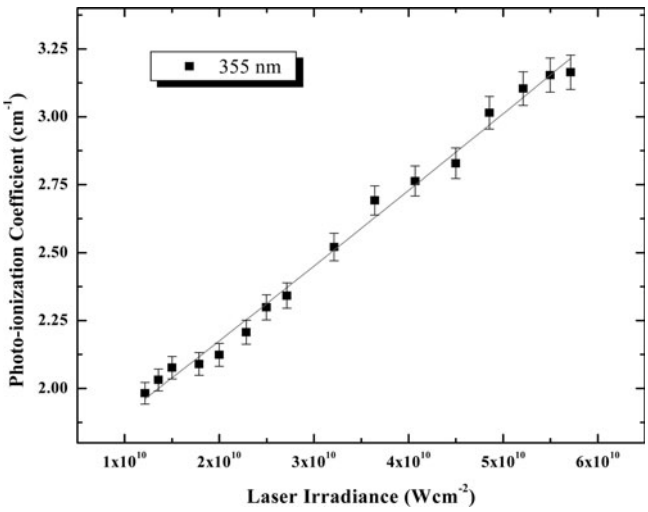

Fig. 8. Variation of the calculated photoionization absorption α_{PI} with the laser irradiance for the 355 nm laser.

https://doi.org/10.1017/S0263034608000062 Published online by Cambridge University Press

duced under low pressure appeared sharper than those produced under an atmospheric pressure. With an increase in the pressure a strong continuum is manifested. Continuum is related to strong collisions between the free electrons and the excited atoms, and ions and the recombination of electrons and ions. With an increase in the ambient gas pressure, the broadening of the spectral lines increases as shown in Figure 9. When the pressure is increased beyond 20 mbar, the confined plasma doesn't emit sharp lines. When the pressure is increased beyond 20 mbar, self absorption has been observed in the resonance lines of Ca I and Ca II. The behavior of the Ca II $^2P_{1/2,3/2} \rightarrow 4s\ ^2S_{1/2}$ resonance lines with the increase in the pressure is shown in Figure 9. Self absorption is evident in the 393.47 nm line. The line peak is fist flattened and then reversed following a dip in the middle of the line (Cowan, 1981; Cremers & Radziemski, 2006). In the case of low pressure, the plasma spreads in a large volume and causes a decrease in the intensity. The electron temperature and number density are affected by the expansion of the plasma. The explanation of the shift and broadening of the spectral lines is the Stark shift, the perturbation resulting from the interaction between the excited radiating state and the external electric field generated from the charge particles such as electrons and ions. The resultant shift is dependent on the external electric field and thus to ions and electrons densities. Although we have not observed any significant shift in the spectral lines but the line broadening is evident. Since the plasma temperature and electron number density are rapidly changing within the nanosecond intervals, the line broadening is highly time dependent. The behavior of the number density and temperature has been studied by varying the ambient gas pressure, which is varied from 3 to 100 mbar. The variation in the temperature is from 11000 to 16300 K, while the number density varies from 6×10^{17} to 2.2×10^{18} cm^{-3}, shown in Figure 10. As the gas pressure is increased, the emission intensity increases depending on the laser energy. With an increase in the ambient gas

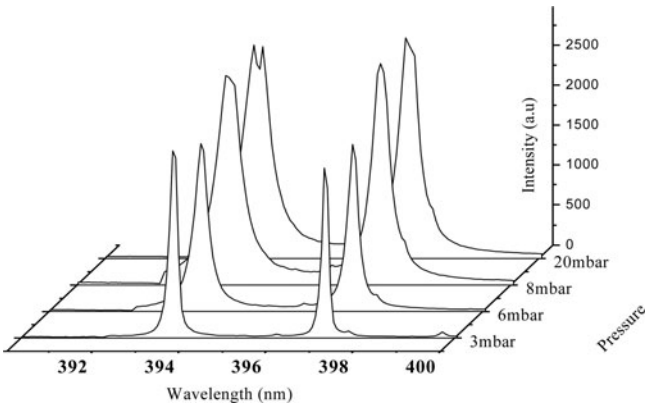

Fig. 9. Variation in the broadening and intensity of the spectral lines as a function of ambient gas pressures. The self absorption in the line profiles of Ca II 4p $^2P_{3/2} \rightarrow 4s\ ^2S_{1/2}$ transition is evident.

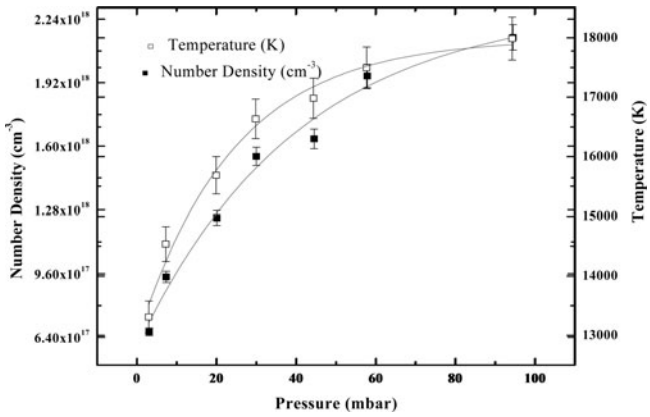

Fig. 10. Variation in the electron temperature and number density as a function of ambient gas pressure.

pressure, an increase in the temperature and number density has been observed. In vacuum, the plasma expands freely while in the presence of ambient gas the plasma is confined to a small region. Hence the ambient gas acts as a damping material to prevent the free expansion of the plume. Thus the expansion rate is reduced and cooling is enhanced. Also the rate of recombination and collisional excitation of the plasma increases with the resulting increase in the line intensities. Laser radiation absorption by the ambient gas in the plasma plume plays a significant role in the target evaporation processes and the spectral emission characteristics. This effect is avoided in our experiments by the tight focusing of the laser beam. Cristoforetti *et al.* (2004) estimated the electron temperature and number density as a function of ambient gas pressure using a Nd:YAG laser at 1064 nm on the brass sample. They observed a decrease in the temperature and number density at an atmospheric pressure due to the energy loss by the plasma as a result of collision with the ambient gas.

4. CONCLUSION

The LIBS method has been successfully applied as an analytical technique for the analysis of calcium using a Nd:YAG laser at its fundamental, second, and third harmonic. The electron temperature and number density is evaluated from the spatially resolved spectrum. Plasma parameters have also been calculated as a function of laser irradiance and ambient gas pressure. The estimated electron impact excitation time is 0.4 ns, short enough to produce an increase in the excited state density. The electrons produced *via* ion beam and PI processes increase the excited state number density. It has been observed from the emission spectrum that the ionic lines of calcium are very strong, and they show self absorption beyond 20 mbar. At 500 mbar besides resonance lines, the self absorption has also been observed in the other transition lines.

https://doi.org/10.1017/S0263034608000062 Published online by Cambridge University Press

ACKNOWLEDGEMENTS

We are grateful to the Quaid-i-Azam University, Islamabad, and Higher Education Commission (HEC) for providing necessary funds to acquire the LIBS equipment. Authors are grateful to HEC for providing the scholarships for the Ph.D. research work.

REFERENCES

Abdellatif, G. & Imam, H. (2002). A study of the laser plasma parameters at different laser wavelengths. *Spectrochim. Acta B* **57**, 1155–1165.

Amoruso, S., Bruzzese, R., Spinelli, N. & Velotta, R. (1999). Characterization of laser-ablation plasmas. *J. Phys. B: At. Mol. Opt. Phys*. **32**, R131–R172.

Asimellis, G., Giannoudakos, A. & Kompitsas, M. (2006). Near-IR bromine laser conduced breakdown spectroscopy detection and ambient gas effects on emission line asymmetric Stark broadening and shift. *Spectrochim. Acta B* **61**, 1270–1278.

Barklem, P.S. & O' Mara Mon, B. (1998). The broadening of strong lines of Ca^{+}, Mg^{+} and Ba^{+} by collisions with neutral hydrogen atoms. *J. Not. Astron. Soc*. **300**, 863–871.

Bashir, S., Rafique, M.S. & Ul-Haq, F. (2007). Laser ablation of ion irradiated CR-39. *Laser Part. Beams* **25**, 181–191.

Body, D. & Chadwick, B.L. (2001). Simultaneous elemental analysis system using laser induced breakdown spectroscopy *Rev. Sci. Instru*. **72**, 1625–1629.

Bogaerts, A., Chen, Z., Gjbels, R. & Vertes, A. (2003). Laser ablation for analytical sampling: What can we learn from modeling? *Spectrochim. Acta B* **58**, 1867–1893.

Bogaerts, A., Chen, Z. & Bleiner, D. (2006). Laser ablation of copper in different background gases: Comparative study by numerical modeling and experiments. *J. Analytical Atomic Spectrometry* **21**, 384–395.

Bustamante, M.F., Rinaldi, C.A. & Ferrero, J.C. (2002). Laser induced breakdown spectroscopy characterization of Ca in a soil depth profile. *Spectrochim. Acta B* **57**, 303–309.

Bussoli, M., Batani, D., Desai, T., Canova, F., Milani, M., Trtica, M., Gakovic, B. & Krousky, E. (2007). Study of laser induced ablation with focused ion beam/scanning electron microscope devices. *Laser Part. Beams* **25**, 121–125.

Bulgakov, A.V. & Bulgakova, N.M. (1998). Gas-dynamic effects of the interaction between a pulsed laser-ablation plume and ambient gas: Analogy with an under expanded jet. *J. Phys. D: Appl. Phys.* **31**, 693–703.

Capitelli, M., Casavola, A., Colonna, G. & De Giacomo, A. (2004). Laser-induced plasma expansion theoretical and experimental aspects. *Spectrochim. Acta B* **59**, 271–289.

Chang, J.J. & Warner, B.E. (1996). Laser-plasma interaction during visible-laser ablation methods. *Appl. Phys. Lett*. **69**, 473– 475.

Chen, Z. & Bogaerts, A. (2005). Laser ablation of Cu and plume expansion into 1 atm ambient gas. *J. Appl. Phys*. **97**, 063305–1–12.

Cowan, R.D. (1981). Detector was approximately placed at the distance of 0.5 mm from the target. *The Theory of Atomic Structure and Spectra.* University of California press.

Colon, C., Hatem, G., Verdugo, E., Ruiz, P. & Campos, J. (1993). Measurement of the Stark broadening and shift parameters for several ultraviolet lines of singly ionized aluminum. *J. Appl. Phys*. **73**, 4752–4758.

Colonna, G., Casavola, A. & Capitelli, M. (2001). Modeling of LIBS plasma expansion. *Spectrochim. Acta B* **56**, 567.

Cristoforetti, G., Legnaioli, S., Palleschi, V., Salvetti, A. & Tognoni, E. (2004). Influence of ambient gas pressure on laser-induced breakdown spectroscopy technique in the parallel double-pulse configuration. *Spectrochimica Acta B* **59**, 1907–1917.

Cremers, D.A. & Radziemski, L.J. (2006). *Handbook of Laser-Induced Breakdown Spectroscopy.* New York: John Wiley & Sons, Ltd.

De Giacomo, A. (2003). Experimental characterization of metallic titanium-laser induced plasma by time and space resolved optical emission spectroscopy. *Spectrochim. Acta B* **58**, 71–83.

D'Couto, G.C. & Babu, S.V. (1994). Heat transfer and material removal in pulsed excimer-laser-induced ablation: Pulse width dependence. *J. Appl. Phys*. **76**, 3052–3058.

Gomes, A., Aubreton, A., Gonzalez, J.J & Vaquie, S. (2004). Experimental and theoretical study of the expansion of metallic vapor plasma produced by laser. *J. Phys. D. Appl. Phys*. **37**, 689–696.

Gornushkin, I.B., King, L.A, Smith, B.W, Omenetto, N. & Winefordner, J.D. (1999). Line broadening mechanisms in the low pressure laser-induced plasma. *Spectrochim. Acta B* **54**, 1207–1271.

Griem, H.R. (1997). *Principles of Plasma Spectroscopy* Cambridge: Cambridge University Press.

Hafez, M.A., Khedr, M.A. Elaksher, F.F. & Gamal, Y.E. (2003). Characterization of Cu plasma produced by a laser interaction with a solid target. *Plasma Sources Sci. Technol*. **12**, 185–198.

Harilal, S.S., Bindhu, C.V., Issac, Riju C., Nampoori, V.P.N. & Vallabhan, C.P.G. (1997). Electron density and temperature measurements in a laser produced carbon plasma. *J. Appl. Phys*. **82**, 2140–2146.

Lam, Y.C., Tran, D.V. & Zheng, H.Y. (2007). A study of substrate temperature distribution during ultrashort laser ablation of bulk copper. *Laser Part. Beams* **25**, 155–159.

Laville, S., Vidal, F., Johnston, T.W., Chaker, M. & Le Drogoff, B. (2004). Modeling the time evolution of laser-induced plasmas for various pulse durations and fluences. *Phys. Plasmas* **11**, 2182–2190.

Marr, G.V. (1968). *Plasma Spectroscopy.* Amstrerdam: Elsevier.

Maravelaki-Kalaitzaki, P., Anglos, D., Kilikolou, V. & Zafiropulos, V. (2001). Compositional characterization of encrustation on marble with laser induced breakdown spectroscopy. *Spectrochim. Acta B* **56**, 887–903.

Martin, P., Trainham, R., Agostini, P. & Petite, G. (1992). Electron and ion emission in high-intensity laser irradiation of aluminum. *Phys. Rev. B* **45**, 69–77.

Miziolek, A.W., Palleschi, V. & Schechter, I. (2006). *Laser Induced Breakdown Spectroscopy Fundamentals and Applications* Cambridge: Cambridge University Press.

Atomic Spectroscopic Data, NIST. http://www.physics.nist.gov/PhysRefdata/contents.html.

Ozaki, T., Bom, L.B.E., Ganeev, R., Kieffer, J.C., Suzuki, M. & Kuroda, H. (2007). Intense harmonic generation from silver ablation. *Laser Part. Beams* **25**, 321–325.

Ortiz, M. & Mayo, R. (2005). Measurement of the Stark broadening for several lines of singly ionized gold. *J. Appl. Phys. B At. Mol. Opt. Phys*. **38**, 3953–3961.

https://doi.org/10.1017/S0263034608000062 Published online by Cambridge University Press

Russo, R.E., Mao, X.L., Liu, H.C., Yoo, J.H. & Mao, S.S. (1999). Time-resolved plasma diagnostics and mass removal during single-pulse laser ablation. *Appl. Phys. A* **69**, S887–S894.

Schaumann, G., Schollmeier, M.S., Rodriguez-Prieto, G., Blazevic, A., Brambrink, E., Geissel, M., Korostiy, S., Pirzadeh, P., Roth, M., Rosmej, F.B., Faenov, A.Y., Pikuz, T.A., Tsigutkin, K., Maron, Y., Tahir, N.A. & Hoffmann, D.H.H. (2005). High energy heavy ion jets emerging from laser plasma generated by long pulse laser beams from the NHELIX laser system at GSI. *Laser Part. Beams* **23**, 503–512.

Schade, W., Bohling, C., Hohmann, K. & Scheel, D. (2006). Laser-induced plasma spectroscopy for mine detection and verification. *Laser and Particle Beams* **24**, 241–247.

Shaikh, N.M., Rashid, B., Hafeez, S., Jamil, Y. & Baig, M. A. (2006*a*). Measurement of electron density and temperature of a laser-induced zinc plasma. *J. Phys. D: Appl. Phys.* **39**, 1384.

Shaikh, N.M., Hafeez, S., Rashid, B., Mahmood, S. & Baig, M.A. (2006*b*). Optical emission studies of the mercury plasma generated by the fundamental, second and third harmonics of a Nd:YAG laser. *J. Phys. D: Appl. Phys.* **39**, 4377–4385.

Shaikh, N.M., Rashid, B., Hafeez, S., Mahmood, S., Saleem, M. & Baig, M.A. (2006*c*). Diagnostics of cadmium plasma produced by laser ablation. *J. Appl. Phys*. **100**, 073102.

Shaikh, N.M, Hafeez, S., Rashid, B. & Baig, M.A. (2007). Spectroscopic studies of laser induced aluminum plasma using fundamental, second and third harmonics of a Nd:YAG laser. *Eur. Phys. J. D*: **44**, 371–379.

Singh, R. K., Holland, O.W. & Narayan, J. (1990). Theoretical model for deposition of superconducting thin films using laser evaporation technique. *J. Appl. Phys*. **68**, 233–247.

Lee, Y., Thiem, T.L., Kim, Gi-Ho T.L., Ye-Yung, T. & Sneddon, J. (1992). Interaction of an excimer-laser beam with metals. Part III: The effect of a controlled atmosphere in laser-ablated plasma emission. *Appl. Spectroscopy* **46**, 1597–1604.

Trusso, S., Barletta, E., Barreca, F., Fazio, E. & Neri, F. (2005). Time resolved imaging studies of the plasma produced by laser ablation of silicon in O_2/Ar atmosphere. *Laser Part. Beams* **23**, 149–153.

Thareja, R.K. & Sharma, D.K. (2006). Reactive pulsed laser ablation: Plasma studies. *Laser Part. Beams* **24**, 311–320.

Veiko, V.P., Shakhno, E.A., Smirnov, V.N., Miaskovski, A.M. & Nikishin, G.D. (2006). Laser-induced film deposition by LIFT: Physical mechanisms and applicat**ions**. *Laser Part. Beams* **24**, 203–209.

Vidal, F., Laville, S., Johnston, T.W., Barthelemy, O., Chaker, M., Le Drogoff, B., Margot, J. & Sabsabi, M. (2001). Numerical simulations of ultrashort laser pulse ablation and plasma expansion in ambient air. *Spectrochim. Acta B* **56**, 973–986.

Wang, Y.-L., Xu, W., Zhou, Y., Chu, L.-Z. & Fu, G.-S. (2007). Influence of pulse repetition rate on the average size of silicon nano-particles deposited by laser ablation. *Laser Part. Beams* **25**, 9–13.

Wieger, V., Strassl, M. & Wintner, E. (2006). Pico- and microsecond laser ablation of dental restorative materials. *Laser Part. Beams* **24**, 41–45.

Whirter, M.RW.P (1965). *Plasma Diagnostic Techniques*, Huddlestone R H & Leonard S.L., New York: Academic Press.

Ying, M., Xia, Y., Sun, Y., Zhao, M., Ma, Y., Liu, X., Li, Y. & Hou, X. (2003). Plasma properties of a laser-ablated aluminum target in air. *Laser Part. Beam* **21**, 97–101.

Zbroniec, L., Sasaki, T. & Koshizaki, N. (2004). Effect of ambient gas laser fluence on the compositional changes in iron oxide particles aggregated films prepared by laser ablation. *Appl. Phys. A* **79**, 1783.

Zeng, X., Mao, S.S., Liu, C., Mao, X., Greif, R. & Russo, R.E. (2003). Plasma diagnostics during laser ablation in a cavity. *Spectrochim. Acta B* **58**, 867–877.

https://doi.org/10.1017/S0263034608000062 Published online by Cambridge University Press